

Communication

Investigation on the Formation of Rare-Earth Metal Phenoxides via Metathesis

Jintao Wang^{1,2}, Qijun Pei¹, Yang Yu¹, Jirong Cui^{1,2}, Shangshang Wang^{1,2}, Khai Chen Tan^{1,2}, Jiaquan Guo^{1,2}, Teng He^{1,2,*} and Ping Chen^{1,2,3}¹ Dalian Institute of Chemical Physics, Chinese Academy of Sciences, Dalian 116023, China² Center of Materials Science and Optoelectronics Engineering, University of Chinese Academy of Sciences, Beijing 100049, China³ State Key Laboratory of Catalysis, Dalian Institute of Chemical Physics, Chinese Academy of Sciences, Dalian 116023, China

* Correspondence: heteng@dicp.ac.cn

Abstract: A number of alkali organometallic complexes with suitable thermodynamic properties and high capacity for hydrogen storage have been synthesized; however, few transition metal–organic complexes have been reported for hydrogen storage. Moreover, the synthetic processes of these transition metal–organic complexes via metathesis were not well characterized previously, leading to a lack of understanding of the metathesis reaction. In the present study, yttrium phenoxide and lanthanum phenoxide were synthesized via metathesis of sodium phenoxide with YCl_3 and $LaCl_3$, respectively. Quasi in situ NMR, UV-vis, and theoretical calculations were employed to characterize the synthetic processes and the final products. It is revealed that the electron densities of phenoxides in rare-earth phenoxides are lower than in sodium phenoxide due to the stronger Lewis acidity of Y^{3+} and La^{3+} . The synthetic process may follow a pathway of stepwise formation of dichloride, monochloride, and chloride-free species. Significant decreases in K-band and R-band absorption were observed in UV-vis, which may be due to the weakened conjugation effect between O and the aromatic ring after rare-earth metal substitution. Two molecular structures, i.e., planar and nonplanar, are identified by theoretical calculations for each rare-earth phenoxide. Since these two structures have very close single-point energies, they may coexist in the materials.

Keywords: rare-earth organometallic complexes; metathesis; yttrium phenoxide; lanthanum phenoxide; hydrogen storage



Citation: Wang, J.; Pei, Q.; Yu, Y.; Cui, J.; Wang, S.; Tan, K.C.; Guo, J.; He, T.; Chen, P. Investigation on the Formation of Rare-Earth Metal Phenoxides via Metathesis. *Inorganics* **2023**, *11*, 115. <https://doi.org/10.3390/inorganics11030115>

Academic Editors: Craig Buckley and Michael A. Beckett

Received: 8 February 2023

Revised: 1 March 2023

Accepted: 7 March 2023

Published: 10 March 2023



Copyright: © 2023 by the authors. Licensee MDPI, Basel, Switzerland. This article is an open access article distributed under the terms and conditions of the Creative Commons Attribution (CC BY) license (<https://creativecommons.org/licenses/by/4.0/>).

1. Introduction

Nowadays, oil and gas are used as the main sources of energy; however, the use of fossil sources leads to significant air pollution and global warming, which has become a huge challenge for the world [1]. To reduce energy consumption and CO_2 emissions from transportation and industries, the search for renewable energy sources is the foremost task [2]. Recently, some renewable energy sources have been used instead of traditional fossil sources; however, renewables such as solar and wind still have limitations, e.g., high cost, low efficiency, less reliability, and poor stability, due to the undesired environmental change. A suitable energy carrier is essential to solve these issues and controllably absorb or release energy. A promising energy carrier is hydrogen [3]. Hydrogen is abundant, combustible, and possesses high energy density compared to other energy sources. Hydrogen can be produced through several methods, including natural gas reforming [4], electrolysis [5], solar-driven [6], and biological processes [7]. Additionally, the hydrogen fuel cell not only transforms chemical energy to electricity with a high conversion (60% against 20% for combustion engines) but also produces water vapor through the chemical reaction between hydrogen and air in the presence of a catalyst. Unfortunately, hydrogen storage is challenging due to the high flammability and low density of the hydrogen gas.

Lack of efficient hydrogen storage methods is one of the bottlenecks for the implementation of hydrogen energy [8–10]. Hydrogen may be absorbed by using material in which hydrogen bonds chemically or by physical absorption on solids, such as metal hydrides, alloys, carbon nanotubes, graphene, borohydrides, and ammonia borane [11]. It was widely accepted that storage of hydrogen in chemical compounds provided a safer and more efficient solution [12,13]. Diverse chemical materials have been developed, such as metal hydrides, complex hydrides, chemical hydrides, liquid organic hydrogen carriers, and so on. Very recently, organometallic complexes, a new family of hydrogen storage materials, were developed [14,15]. The dehydrogenation thermodynamics of H-rich organometallic complexes can be rationally tuned thanks to the electron-donating abilities of alkali metals, allowing reversible hydrogen uptake and release at ambient conditions from a thermodynamic point of view. A number of alkali organometallic complexes have been synthesized, including phenoxides [16], anilines [17], pyrrolides [18], imidazolides [19], indolides [20], azaindolides [20], and carbazolides [19]. However, slow hydrogenation and dehydrogenation kinetics were observed even in the presence of transition metal catalysts at high temperatures, which may in part be due to the sluggish mass transfer in solid-state catalysis. Essentially, excellent contact between catalysts and substrates plays a vital role, where an ideal scenario is to fabricate a molecule that consists of transition metal and a hydrogen storage portion. Fortunately, organometallic complexes that have both metal cations and organic groups in one molecule provide a suitable platform to build such molecules. In this way, the hydrogenation and dehydrogenation of fabricated transition metal–organic complexes may be realized for hydrogen storage in the absence of catalysts. However, few transition metal–organic complexes for hydrogen storage have been reported.

Rare earth (RE) chemistry has gained increased attention in recent decades due to its application in catalysis, metallurgy, glass, hydrogen storage, superconductor, and so on [21,22]. Usually, RE elements are found in a variety of accessory minerals, such as phosphate, carbonates, fluorides, and silicates [23]. RE elements have been studied in the field of hydrogen storage in the last several decades. RE hydrides can reversibly absorb and desorb hydrogen. Although the RE hydrides are not good hydrogen storage materials due to their low hydrogen capacity and high dehydrogenation temperature, alloys consisting of RE metals and other metals (i.e., alkali metals, alkali earth metals, transition metals) are well known to exhibit high volumetric hydrogen capacity [24]. To enhance the hydrogen storage properties, a number of studies exploring new RE-based alloys and hydrides have been conducted using many methods, such as melting and ball milling. Typically, LaNi_5 can absorb hydrogen to form LaNi_5H_6 and release hydrogen upon heating in ambient conditions [25]. Moreover, thanks to the advances in anaerobic manipulation techniques and ligand designs, lanthanide metals (except radioactive promethium) and yttrium can form numerous molecular species with organic ligands [26]. Among them, the unique series of compounds of aliphatic alkoxides and aryloxides with the REs have come to the forefront for their unique properties and applications in the preparation of organometallics [22]. For instance, RE aryloxides can be employed as precursors to prepare new complexes, i.e., protonolysis reaction of 1-phenyl-3-N-(p-methoxyphenylimino)-1-butanone (HL) with RE aryloxides $[\text{RE}(\text{OAr})_3(\text{THF})_n]$ ($\text{ArO} = 2,6\text{-Bu}^t_2\text{-4-MeC}_6\text{H}_2\text{O}$) in THF can give mononuclear lanthanide aryloxides $\text{L}_2\text{RE}(\text{OAr})(\text{THF})_n$ ($\text{RE} = \text{Y, Nd}$) [27]. Another application of $\text{RE}(\text{OAr})_3(\text{THF})_n$ is to react with organolithium reagents to prepare new RE metal–organic complexes [28]. Additionally, RE cations, such as Eu^{3+} and Tb^{3+} , in which luminescence results from the $4f \rightarrow 4f$ and $4f \rightarrow 5d$ transitions, give rise to relatively broad absorption and high emission intensities, and RE aryloxides have become a new type of tunable and energy-efficient luminophores [29]. Usually, RE aryloxides are obtained from the metathesis of RE halides and aryloxides [30,31]. Through this method, diverse RE aryloxides have been developed; however, the synthetic processes are not well characterized, leading to a lack of understanding of the metathesis reaction.

Therefore, in the present study, two rare-earth organic complexes, i.e., yttrium phenoxide and lanthanum phenoxide, were synthesized via metathesis reaction. Quasi in

situ nuclear magnetic resonance (NMR) and ultraviolet-visible (UV-vis) methods were employed to characterize the formation processes and electronic states of these two phenoxides. The molecular structures were predicated by theoretical calculations. Meanwhile, attempts at hydrogenation of yttrium and lanthanum phenoxides for hydrogen storage were conducted.

2. Results

2.1. Syntheses of Rare-Earth Metal Phenoxides

In our previous investigations, alkali organometallic complexes were synthesized via the reaction of alkali metal hydrides and organic compounds that have protic H, releasing one equivalent H_2 at the same time [14]. Accordingly, carbazole and indole were employed to react with rare-earth metal hydrides (YH_3 and LaH_3) in the present study; however, no reaction was observed. Even phenol, with more protic H than that of carbazole and indole, did not react with YH_3 and LaH_3 upon intensive ball milling. Therefore, a metathesis reaction was employed for the synthesis of yttrium phenoxide ($Y(OPh)_3$) and lanthanum phenoxide ($La(OPh)_3$). A schematic diagram of the preparation method is shown in Figure 1. First, sodium phenoxide ($NaOPh$) was prepared via the reaction of phenol and sodium hydride via ball mill, releasing one equivalent hydrogen. Then, sodium phenoxide reacted with corresponding chlorides (YCl_3 and $LaCl_3$) in ethanol, generating $Y(OPh)_3$ and $La(OPh)_3$, respectively, as shown in R1 and R2. Since $NaCl$ has low solubility in ethanol, the products $Y(OPh)_3$ and $La(OPh)_3$ can be facily separated through filtration. After evaporation of ethanol at $200\text{ }^\circ\text{C}$, target products without organic ligand were obtained.

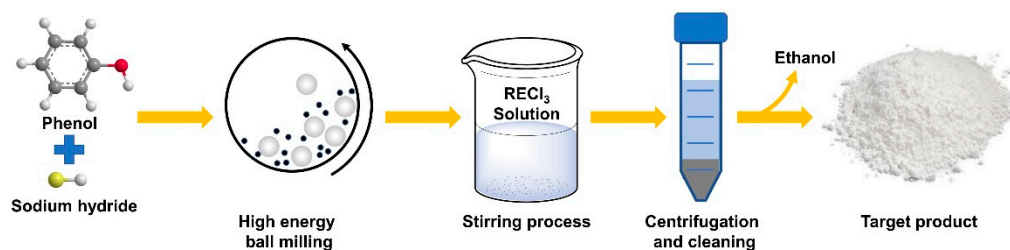
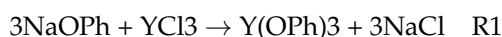


Figure 1. Schematic diagram of preparation method for rare-earth organic compounds.

The formation of $NaCl$ from R1 and R2 in the precipitates was confirmed by X-ray diffraction (XRD), as shown in Figure 2a. The weights of precipitates from both reactions were consistent with the theoretical values of the $NaCl$ produced, indicating almost all the Na and Cl were removed from the solution. Furthermore, the Na species could hardly be observed from ^{23}Na NMR solutions, further confirming that most of the $NaCl$ was precipitated (Figure S1). However, both $Y(OPh)_3$ and $La(OPh)_3$ from the distillations exhibited a few broad diffraction peaks after removing the solvent (Figure 2b), demonstrating the amorphous state of the two samples, which is consistent with the transmission electron microscopy (TEM) images (Figure 2c). The absence of $NaOPh$ in the XRD patterns also suggests its full conversion to La and Y phenoxides. Fourier-transform infrared (FT-IR) characterizations on these two samples demonstrated similar spectra as $NaOPh$, suggesting the retention of its phenol group (Figure S2). The appearance of vibrations at 583 and 566 cm^{-1} in $Y(OPh)_3$ and $La(OPh)_3$ indicate the formation of $Y-O$ and $La-O$ bonds and the replacement of Na by Y and La , respectively [32–34]. It was shown that all the ethanol solvent had been removed under vacuum at $200\text{ }^\circ\text{C}$ in the solid products, as evidenced by 1H NMR in $DMSO-d_6$ (Figure S3). Elemental analysis results for the amorphous $Y(OPh)_3$ showed that the ratio of $Y:C$ was ca. 1:18, confirming the composition of $Y(OPh)_3$.

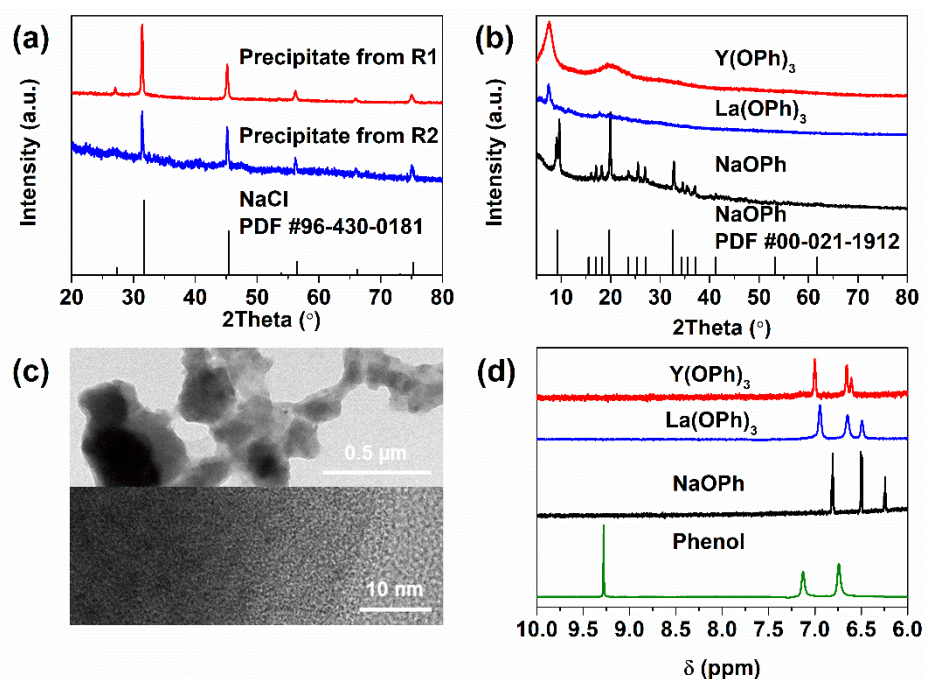


Figure 2. (a) The XRD patterns of the precipitates from R1 and R2. (b) The XRD patterns of $Y(OPh)_3$ and $La(OPh)_3$ compared with NaOPh. (c) Morphologies of $Y(OPh)_3$ observed by TEM. (d) 1H NMR spectra of $Y(OPh)_3$ and $La(OPh)_3$ compared with NaOPh and phenol, respectively.

NMR was employed to characterize the two samples in comparison with phenol and sodium phenoxide. It was shown that signals of both $Y(OPh)_3$ and $La(OPh)_3$ in 1H NMR shifted downfield compared with NaOPh, confirming the formation of new compounds. Their chemical shifts were different from those of phenol, excluding the hydrolysis/alcoholysis of sodium phenoxide to phenol. Compared with the signals of phenol, all signals of NaOPh, $Y(OPh)_3$, and $La(OPh)_3$ moved upfield and followed the order of $NaOPh > La(OPh)_3 > Y(OPh)_3$, which follows the Lewis acidity of the cations, i.e., $Na^+ (0.159) < La^{3+} (0.343) < Y^{3+} (0.393)$ [35]. ^{13}C NMR spectra also revealed the impact of metathesis (Figure S4), i.e., the signals of C atoms at 1 and 2 sites in NaOPh moved to the high field and other signals to the low field upon replacing Na with Y cation. These results clearly demonstrated that rare-earth cations had successfully substituted the sodium cations in NaOPh, yielding $Y(OPh)_3$ and $La(OPh)_3$. However, no single crystal was obtained, leading to a lack of structural information about these two compounds. The crystal structure of ligand-free RE phenoxide has seldom been reported in the literature [21,36].

2.2. Characterizations

Although the synthesis of Y and La phenoxides has been reported previously, the synthetic processes are not well characterized, leading to a lack of understanding of the metathesis reaction. To get an understanding of the transformation processes from NaOPh to $Y(OPh)_3$ and $La(OPh)_3$, quasi in situ NMR was performed, where NaOPh was gradually added to pristine YCl_3 and $LaCl_3$ solutions. For pristine NaOPh in Figure 3a, chemical shifts at 6.81, 6.50, and 6.24 ppm were assigned to β -H, α -H, and γ -H in the phenoxide ring, respectively. When one equivalent NaOPh was added into YCl_3 , chemical shifts at 6.95, 6.60, and 6.55 ppm were observed, which were different from those of pristine NaOPh, indicating the occurrence of cation exchange. When the molar ratio of NaOPh to YCl_3 increased from 1 to 1.2, 1.5, 2, and 3, all the signals shifted slightly downfield, suggesting the gradual formation of dichloride, monochloride, and chloride-free $YCl_n(OPh)_{3-n}$ ($0 \leq n \leq 3$) species. The elemental analysis results on the products of 1–1, 1–2 and 1–3 showed that the ratios of Y:C were 1:6, 1:12, and 1:18, respectively, confirming the formation of dichloride, monochloride, and chloride-free species. The slight downfield shift may be due to $Y^{\delta+}$

cations accepting fewer electrons from each phenoxide when more sodium phenoxide was added. The molar ratio of 1:3 yielded the target product $Y(OPh)_3$. When the molar ratio of NaOPh to YCl_3 reached 1:6, an obvious shift upfield was obtained, located between that of $Y(OPh)_3$ and NaOPh, indicating that a mixture of these two compounds may be formed.

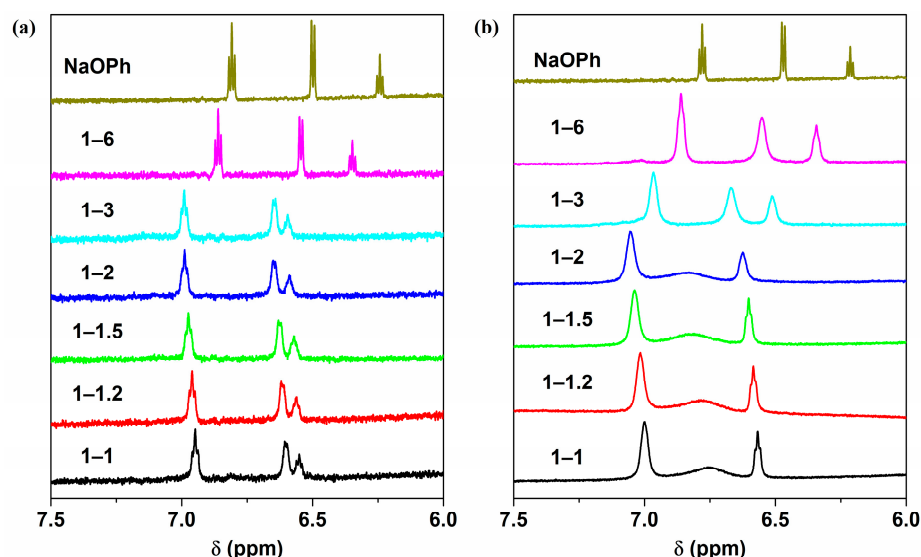


Figure 3. 1H NMR characterizations on the reactions of (a) YCl_3 - $nNaOPh$ and (b) $LaCl_3$ - $nNaOPh$ ($n = 1-6$) with the increase in molar ratio of NaOPh, respectively.

For the $LaCl_3$ case in Figure 3b, it is similar to that of YCl_3 , i.e., the chemical shifts gradually moved downfield at the initial stage and then upfield when the molar ratio of NaOPh was higher than 3. It is worth mentioning that the signal of α -H at ~ 6.67 ppm became significantly broadened when the ratio of NaOPh was less than 3. This may be due to (1) activation of *ortho*-H, (2) electrostatic cation- π interactions, or (3) fast transition between monomeric species and oligomeric products.

Apart from the NMR characterizations, UV-vis absorption spectra were also collected on the same samples. As shown in Figure 4, YCl_3 and $LaCl_3$ solutions showed negligible absorption in the range of 200 to 400 nm, whereas the pristine sodium phenoxide exhibited strong absorption peaks at 218, 238, 273, and 295 nm in ethanol solution. When one equivalent sodium phenoxide was added to $YCl_3/LaCl_3$ solutions, the absorption peaks at 218 and 273 nm that were assigned to the E-band and B-band due to the $\pi \rightarrow \pi^*$ transition in aromatic compounds, respectively, were retained, while the absorption bands at 238 and 295 nm disappeared. The absorption band at 238 nm is usually referred to as the K-band due to $\pi \rightarrow \pi^*$ transition in aromatic compounds that have an unsaturated functional group conjugated with the aromatic ring, while the absorption at 295 nm is the R-band generated by $n \rightarrow \pi^*$ transition of functional group that attaches to the aromatic ring and contains a nonbonding pair of electrons [37,38]. It was reported that both the K-band and R-band are particularly sensitive to the substituent group of the aromatic ring [39]. The disappearance of bands at 238 and 295 nm on UV-vis examination showed the substitution of sodium by rare-earth metals, agreeing well with the stronger Lewis acidity of La^{3+} and Y^{3+} compared with Na^+ [35]. Meanwhile, it also indicated that the conjugation effect between O and the aromatic ring may be weakened after Y/La substitution. When the ratio of NaOPh to $YCl_3/LaCl_3$ was lower than 3, all the spectra exhibited similar profiles. These two absorption bands at 238 nm and 295 nm grew gradually when the ratio of sodium phenoxide to $YCl_3/LaCl_3$ was higher than 3, showing the coexistence of NaOPh in the solutions.

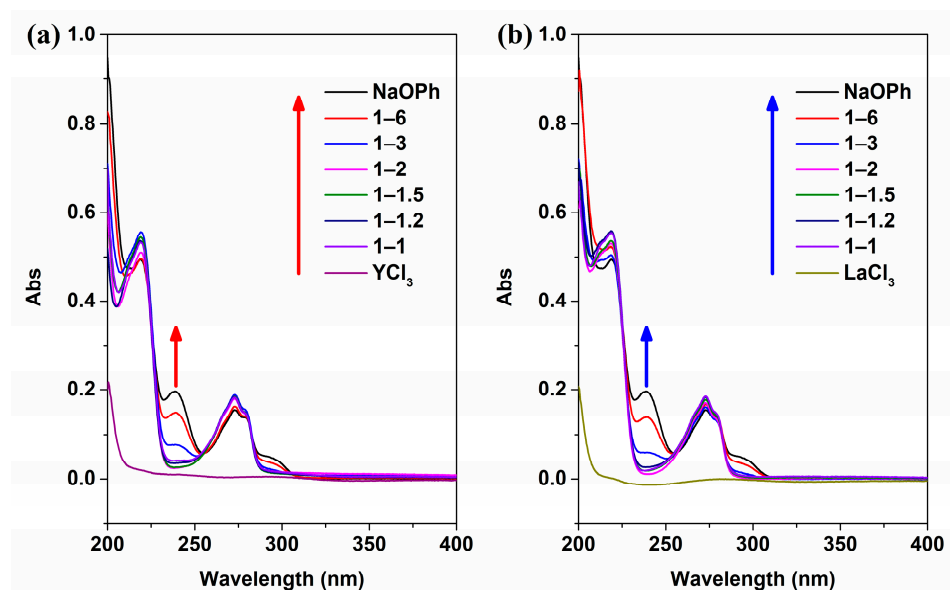


Figure 4. UV-vis characterizations of the reactions of (a) $\text{YCl}_3\text{-nNaOPh}$ and (b) $\text{LaCl}_3\text{-nNaOPh}$ ($n = 1\text{--}6$) with the increase in molar ratio of NaOPh.

2.3. Molecular Structures

Due to the amorphous states, molecular structures of Y(OPh)_3 and La(OPh)_3 were investigated at the B3LYP/def2TZVP level of theory [40,41]. Two initial geometries (parallel and vertical) were proposed and optimized with C3 symmetry due to three identical phenoxide rings that were proved by ^1H and ^{13}C NMR results (Figure 2d and Figure S4). For Y(OPh)_3 , two optimized structures, i.e., planar and nonplanar configurations (Figure 5), were obtained due to the different initial configurations (Figure S5). In the nonplanar configuration, three phenoxide planes connect to the Y center via Y–O bonds and exhibit a dihedral angle of 14.85° to each other, similar to ordered electric fans (Figure 5b and side view in Figure S5). However, the three phenoxides were on the same plane in the planar structure (Figure 5a and Figure S5). The single-point energy of the nonplanar structure was 0.4634 kJ/mol lower than that of the planar one, indicating the nonplanar configuration was more stable, which may be due to intramolecular steric repulsive forces among phenoxide rings. Since these two structures have very close single-point energies, they may coexist during the synthesis and randomly stack via the interactions of van der Waals forces and cation– π and π – π conjugates. Therefore, it is not surprising to obtain weak diffraction peaks in the XRD patterns. The highest occupied molecular orbitals (HOMOs) and lowest unoccupied molecular orbitals (LUMOs) were also calculated based on the two configurations (Figure 5 and Table S1). It can be seen that the LUMOs of the two Y(OPh)_3 structures are located on the metal, whereas the HOMOs are delocalized over benzene rings and oxygens. The gaps between LUMO and HOMO of the planar and nonplanar structures of Y(OPh)_3 are about 3.5914 eV and 3.5734 eV, respectively, which is consistent with the results of the UV-vis spectra, where no absorption in the visible range was observed. The calculated molecular structures of La(OPh)_3 were similar to those of Y(OPh)_3 , and the results can be found in the Supporting Information (Figure S6 and Table S2). Compared with Y(OPh)_3 , the positive charge of La cation in the La(OPh)_3 was higher than the Y cation in Y(OPh)_3 and the oxygen element in the La(OPh)_3 had higher negative charge, which may have been caused by the stronger electron-donating ability of La (Supplementary Tables S1 and S2).

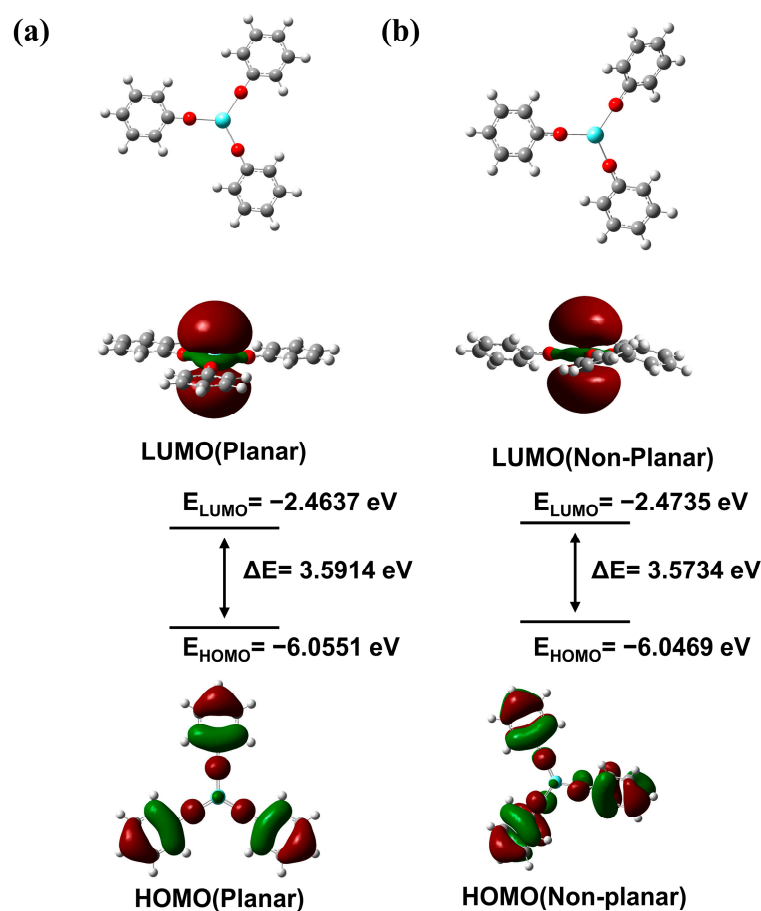


Figure 5. (a,b) Planar and nonplanar structures, LUMOs and HOMOs, and energy gaps between LUMO and HOMO of Y(OPh)_3 , respectively. Black: C; red: O; white: H; greenish-blue: Y.

Given the successful syntheses of Y(OPh)_3 and La(OPh)_3 and their thermal stability (Figure S7), we attempted to hydrogenate these two materials at 100 °C under 70 bar H_2 . However, negligible conversion was observed for both samples, which may be constrained by the difficulty in hydrogen activation due to the full coordination of rare-earth cations. Although there were some reports about the synthesis of Y(III) and La(III) phenoxides previously, there are differences between the previous work and the present research. Table S3 summarizes the differences between previous work and the present study. First, organic ligands (such as THF) are usually needed for the crystal structures of Y and La phenoxides. However, all the organic solvents/ligands were removed in the present study for the purpose of hydrogen storage. Second, the synthetic processes of Y and La phenoxides are not well characterized, leading to a lack of understanding of the metathesis reaction. In the present study, Y and La phenoxides were synthesized via metathesis reaction. Quasi in situ NMR and UV-vis methods were employed to characterize the formation processes in detail. Third, phenoxide without a substituted group was employed in the present study; however, substituted phenoxides were used to synthesize the phenoxide derivatives of Y and La salts previously.

3. Materials and Methods

3.1. Material and Characterization

Commercial phenol (99.5%, TCI, Tokyo, Japan), sodium hydride (90%, Aldrich, Saint Louis, United States), carbazole (95%, Alfa Aesar, Ward Hill, United State), indole (99%, Aldrich, Saint Louis, United States), yttrium metal (99.9%, ACMEC, Shanghai, China), lanthanum metal (99.5%, Aladdin, Shanghai, China), yttrium chloride (99.9%, Alfa Aesar,

Tewksbury, United State), and lanthanum chloride (99.99%, Alfa Aesar) were all stored in a glove box and used without further purification. Anhydrous ethanol (Macklin, Shanghai, China) was used after water removal with a molecular sieve. All the experiments were conducted in a glove box filled with purified argon with <0.1 ppm H_2O and O_2 concentrations. To synthesize sodium phenoxide, a mixture of 0.01 mol sodium hydride and 0.01 mol phenol was put into a 180 mL stainless steel receptacle and ball-milled for 8 h at $200 \text{ r}\cdot\text{min}^{-1}$ accordingly [16]. Yttrium phenoxide and lanthanum phenoxide were synthesized by metathesis reaction. Yttrium chloride (195.5 mg, 1.0 mmol) and sodium phenoxide (355.5 mg, 3.0 mmol) were added into a 50 mL conical flask, then 25 mL anhydrous ethanol was added and stirred at a rate of $300 \text{ r}\cdot\text{min}^{-1}$ at room temperature. After 24 h, the white precipitation was filtered out. Then, the solution was transferred to a glass bottle in the glovebox for evaporation to obtain a powder sample. The powder sample was heated at 200°C in vacuum overnight to complete removal of ethanol, and yttrium phenoxide was obtained. Similarly, the lanthanum phenoxide was prepared by the reaction of lanthanum chloride with sodium phenoxide in anhydrous ethanol with the same method. YH_3 was prepared by direct hydrogenation of Y-metal basis at 350°C under 4 MPa H_2 pressure for 12 h [42,43]. LaH_3 was prepared by a similar method. YH_3 and LaH_3 were ball-milled to powder in 15 bar H_2 atmosphere with a rotating speed of $200 \text{ r}\cdot\text{min}^{-1}$.

XRD patterns were collected on a PANalytical X'pert diffractometer equipped with Cu $\text{K}\alpha$ radiation (40 KV, 40 mA) for phase identification. The test samples were loaded in a homemade sample cell covered with KAPTON film to avoid air and moisture contamination. Temperature-programmed desorption–mass spectrometry (TPD-MS) using purified argon as a carrier gas was conducted in a custom-made reactor. The samples were heated at a rate of $2^\circ\text{C}/\text{min}$ and the gaseous species H_2 , H_2O , CO_2 , CH_4 , and C_2H_6 were monitored using online MS (Hiden, Cheshire, UK).

Solution NMR spectroscopy was recorded on a Bruker AVANCE 700 MHz NMR spectrometer (11.7 T) at ambient temperature. Liquid ^1H and ^{13}C NMR spectra were characterized with DMSO as the deuterated solvent. For ^1H NMR and UV-vis characterizations, yttrium chloride was dissolved in 25 mL anhydrous ethanol solution, and sodium phenoxide with molar ratios of 1, 1.2, 1.5, 2, 3, and 6 equivalent to YCl_3 was added under a stirring rate of $300 \text{ r}\cdot\text{min}^{-1}$ at room temperature. A small amount of solution in each step was taken out for characterizations. UV-vis spectra were measured with a JASCO V-750 spectrophotometer. All prepared solutions were diluted with anhydrous ethanol before UV-vis tests. The pristine yttrium chloride and sodium phenoxide were also dissolved in anhydrous ethanol and characterized for comparison. The formation of lanthanum phenoxide was characterized by the same process. Liquid ^{23}Na NMR spectra were obtained on a Bruker AVANCE 400 MHz NMR spectrometer at room temperature and $\text{DMSO-}d_6$ was used as a deuterated reagent.

TEM images were obtained on a Tecnai G2 F30 S-Twin transmission electron microscope (FEI Company, Hillsboro, United States). The sample was dispersed in cyclohexane and dropped on a carbon-coated copper TEM grid. FT-IR spectra were recorded on a TENSOR II infrared spectrometer.

3.2. Computational Methods

Density functional theory (DFT) calculations were carried out using the Gaussian09 suite of programs [44]. The theoretical geometry of each molecule was optimized at the level of B3LYP/def2TZVP. Geometry optimizations were tested by frequency analysis to ensure that each geometry corresponded to a true local minimum. Natural population analysis was performed to obtain the NBO charges [45]. The GaussView 5 program was used to draw contour plots of HOMOs and LUMOs.

4. Conclusions

In summary, both yttrium phenoxide and lanthanum phenoxide were successfully prepared via metathesis of sodium phenoxide with YCl_3 and LaCl_3 , respectively. NMR

and UV-vis results were used to characterize the detailed process of the replacement of Na cation by Y and La cations, which revealed less electron density in the phenoxide ring and significant decrease in K-band and R-band absorption after metathesis due to the stronger Lewis acidity of Y^{3+} and La^{3+} than Na^+ . The synthetic process may follow a pathway of stepwise formation of dichloride, monochloride, and chloride-free species. Although the crystal structure of $Y(OPh)_3$ and $La(OPh)_3$ are unknown due to the amorphous state of the two samples, DFT calculations were attempted in order to understand the molecular structure and the effect caused by cationic replacement on the organic rings. Two molecular structures, i.e., planar and nonplanar, were identified for each rare-earth phenoxide. The cationic replacement changes the energy gap between LUMO and HOMO and the electron density located at phenoxide rings. Although the hydrogenation of these rare-earth phenoxides was not successful, it is needed to carry out further research. Candidates such as 1-naphthalenol, thiophenol, indole, and imidazole could be investigated in the future, which would obviously broaden the current scope of hydrogen storage systems. More importantly, apart from Y and La, other RE elements are well worthy of attention due to the existence of electrons in their 4f orbitals. Therefore, these rare-earth organic compounds may have potential applications in other areas, such as organic chemistry, catalysis, optical devices, and so on.

Supplementary Materials: The following supporting information can be downloaded at <https://www.mdpi.com/article/10.3390/inorganics11030115/s1>. Figure S1: Liquid ^{23}Na NMR characterizations on the reaction of $YCl_3 \cdot nNaOPh$ ($n = 1, 1.5, 3$); Figure S2: FT-IR spectra of yttrium phenoxide and lanthanum phenoxides; Figure S3: 1H NMR spectra of $Y(OPh)_3$ and $La(OPh)_3$ after removing solvent; Figure S4: ^{13}C NMR of $Y(OPh)_3$ compared with $NaOPh$; Figure S5: Initial geometries and optimized geometries of yttrium phenoxide; Figure S6: Initial geometries and optimized geometries of lanthanum phenoxide; Figure S7: TPD-MS results of yttrium phenoxide and lanthanum phenoxide; Table S1: Single-point energies of two optimized structures of $Y(OPh)_3$; Table S2: Single-point energies of two optimized structures of $La(OPh)_3$; Table S3: Comparison of $Y(III)$ and $La(III)$ phenoxides between the present study and previous research.

Author Contributions: Conceptualization, J.W., Q.P. and Y.Y.; methodology, J.W., J.C. and S.W.; software, J.W.; validation, J.W., K.C.T. and J.G.; formal analysis, J.W.; investigation, J.W.; writing—original draft preparation, J.W.; writing—review and editing, J.W., T.H. and P.C.; project administration, T.H. and P.C.; funding acquisition, T.H. and P.C. All authors have read and agreed to the published version of the manuscript.

Funding: This work was supported by the National Key R&D Program of China (2019YFE0103600), National Natural Science Foundation of China (21875246, 52171226), and Joint Fund of the Yulin University and Dalian National Laboratory for Clean Energy (Grant YLU-DNL, Fund 2021010), and Liaoning Revitalization Talents Program (XLYC2002076).

Data Availability Statement: The data presented in this study are available on reasonable request from the corresponding author.

Conflicts of Interest: The authors declare no conflict of interest.

References

1. Amin, M.; Shah, H.H.; Fareed, A.G.; Khan, W.U.; Chung, E.; Zia, A.; Rahman Farooqi, Z.U.; Lee, C. Hydrogen Production through Renewable and Non-Renewable Energy Processes and Their Impact on Climate Change. *Int. J. Hydrogen Energy* **2022**, *47*, 33112–33134. [[CrossRef](#)]
2. Jiang, W.; Chen, Y.; Hu, M.; Zeng, C.; Liang, C. Rare Earth-Mg-Ni-Based Alloys with Superlattice Structure for Electro-chemical Hydrogen Storage. *J. Alloys Compd.* **2021**, *887*, 161381. [[CrossRef](#)]
3. Osman, A.I.; Mehta, N.; Elgarahy, A.M.; Hefny, M.; Al-Hinai, A.; Al-Muhtaseb, A.a.H.; Rooney, D.W. Hydrogen Production, Storage, Utilisation and Environmental Impacts: A Review. *Environ. Chem. Lett.* **2022**, *20*, 153–188. [[CrossRef](#)]
4. El Hajj Chehade, A.M.; Daher, E.A.; Assaf, J.C.; Riachi, B.; Hamd, W. Simulation and Optimization of Hydrogen Production by Steam Reforming of Natural Gas for Refining and Petrochemical Demands in Lebanon. *Int. J. Hydrogen Energy* **2020**, *45*, 33235–33247. [[CrossRef](#)]

5. Khan, M.A.; Al-Attas, T.; Roy, S.; Rahman, M.M.; Ghaffour, N.; Thangadurai, V.; Larter, S.; Hu, J.; Ajayan, P.M.; Kibria, M.G. Seawater Electrolysis for Hydrogen Production: A Solution Looking for a Problem? *Energy Environ. Sci.* **2021**, *14*, 4831–4839. [[CrossRef](#)]
6. Sultanov, F.; Daulbayev, C.; Bakbolat, B.; Daulbayev, O.; Bigaj, M.; Mansurov, Z.; Kuterbekov, K.; Bekmyrza, K. Aligned Composite SrTiO₃/PAN Fibers as 1D Photocatalyst Obtained by Electrospinning Method. *Chem. Phys. Lett.* **2019**, *737*, 136821. [[CrossRef](#)]
7. Akhlaghi, N.; Najafpour-Darzi, G. A Comprehensive Review on Biological Hydrogen Production. *Int. J. Hydrogen Energy* **2020**, *45*, 22492–22512. [[CrossRef](#)]
8. Schlapbach, L.; Züttel, A. Hydrogen-Storage Materials for Mobile Applications. *Nature* **2001**, *414*, 353–358. [[CrossRef](#)]
9. He, T.; Pachfule, P.; Wu, H.; Xu, Q.; Chen, P. Hydrogen Carriers. *Nat. Rev. Mater.* **2016**, *1*, 16059. [[CrossRef](#)]
10. Lin, H.-J.; Li, H.-W.; Shao, H.; Lu, Y.; Asano, K. In Situ Measurement Technologies on Solid-State Hydrogen Storage Materials: A Review. *Mater. Today Energy* **2020**, *17*, 100463. [[CrossRef](#)]
11. Daulbayev, C.; Lesbayev, B.; Bakbolat, B.; Kaidar, B.; Sultanov, F.; Yeleuov, M.; Ustayeva, G.; Rakhymzhan, N. A Mini-Review on Recent Trends in Prospective Use of Porous 1D Nanomaterials for Hydrogen Storage. *S. Afr. J. Chem. Eng.* **2022**, *39*, 52–61. [[CrossRef](#)]
12. Yang, J.; Sudik, A.; Wolverton, C.; Siegel, D.J. High Capacity Hydrogen Storage Materials: Attributes for Automotive Applications and Techniques for Materials Discovery. *Chem. Soc. Rev.* **2010**, *39*, 656–675. [[CrossRef](#)] [[PubMed](#)]
13. Yadav, M.; Xu, Q. Liquid-Phase Chemical Hydrogen Storage Materials. *Energy Environ. Sci.* **2012**, *5*, 9698–9725. [[CrossRef](#)]
14. He, T.; Cao, H.; Chen, P. Complex Hydrides for Energy Storage, Conversion, and Utilization. *Adv. Mater.* **2019**, *31*, 1902757. [[CrossRef](#)]
15. He, T.; Cao, H.; Chen, P. The Roles of Alkali/Alkaline Earth Metals in the Materials Design and Development for Hydrogen Storage. *Acc. Mater. Res.* **2021**, *2*, 726–738. [[CrossRef](#)]
16. Yu, Y.; He, T.; Wu, A.; Pei, Q.; Karkamkar, A.; Autrey, T.; Chen, P. Reversible Hydrogen Uptake/Release over a Sodium Phenoxide–Cyclohexanolate Pair. *Angew. Chem. Int. Ed.* **2019**, *58*, 3102–3107. [[CrossRef](#)]
17. Jing, Z.; Yu, Y.; Chen, R.; Tan, K.C.; He, T.; Wu, A.; Pei, Q.; Chua, Y.S.; Zheng, D.; Zhang, X.; et al. Sodium Anilide–Cyclohexylamide Pair: Synthesis, Characterization, and Hydrogen Storage Properties. *Chem. Commun.* **2020**, *56*, 1944–1947. [[CrossRef](#)]
18. Jing, Z.; Tan, K.C.; He, T.; Yu, Y.; Pei, Q.; Wang, J.; Wu, H.; Chen, P. Synthesis, Characterization, and Crystal Structure of Lithium Pyrrolide. *Acta Phys.-Chim. Sin.* **2021**, *37*, 2009039. [[CrossRef](#)]
19. Tan, K.C.; Yu, Y.; Chen, R.; He, T.; Jing, Z.; Pei, Q.; Wang, J.; Chua, Y.S.; Wu, A.; Zhou, W.; et al. Metallo-N-Heterocycles—A New Family of Hydrogen Storage Material. *Energy Storage Mater.* **2020**, *26*, 198–202. [[CrossRef](#)]
20. Jing, Z.; Yuan, Q.; Yu, Y.; Kong, X.; Tan, K.C.; Wang, J.; Pei, Q.; Wang, X.-B.; Zhou, W.; Wu, H.; et al. Developing Ideal Metalorganic Hydrides for Hydrogen Storage: From Theoretical Prediction to Rational Fabrication. *ACS Mater. Lett.* **2021**, *3*, 1417–1425. [[CrossRef](#)]
21. Boyle, T.J.; Ottley, L.A.M. Advances in Structurally Characterized Lanthanide Alkoxide, Aryloxide, and Silyloxide Compounds. *Chem. Rev.* **2008**, *108*, 1896–1917. [[CrossRef](#)] [[PubMed](#)]
22. Ortu, F. Rare Earth Starting Materials and Methodologies for Synthetic Chemistry. *Chem. Rev.* **2022**, *122*, 6040–6116. [[CrossRef](#)]
23. Balaram, V. Rare Earth Elements: A Review of Applications, Occurrence, Exploration, Analysis, Recycling, and Environmental Impact. *Geosci. Front.* **2019**, *10*, 1285–1303. [[CrossRef](#)]
24. Lin, H.-J.; Lu, Y.-S.; Zhang, L.-T.; Liu, H.-Z.; Edalati, K.; Révész, Á. Recent Advances in Metastable Alloys for Hydrogen Storage: A Review. *Rare Met.* **2022**, *41*, 1797–1817. [[CrossRef](#)]
25. Sato, T.; Saitoh, H.; Utsumi, R.; Ito, J.; Nakahira, Y.; Obana, K.; Takagi, S.; Orimo, S.I. Hydrogen Absorption Reactions of Hydrogen Storage Alloy LaNi₅ under High Pressure. *Molecules* **2023**, *28*, 1256. [[CrossRef](#)]
26. Huggins, M.L. Electronic Structures of Atoms. *J. Phys. Chem.* **1922**, *26*, 601–625. [[CrossRef](#)]
27. Xia, Q.; Cui, Y.; Yuan, D.; Wang, Y.; Yao, Y. Synthesis and Characterization of Lanthanide Complexes Stabilized by N-Aryl Substituted β-Ketoiminato Ligands and Their Application in the Polymerization of Rac-Lactide. *J. Organomet. Chem.* **2017**, *846*, 161–168. [[CrossRef](#)]
28. Nie, K.; Han, Y.; Wang, C.; Cheng, X. Rare-Earth Metal-Catalyzed Hydroboration of Unsaturated Compounds. *Appl. Organomet. Chem.* **2022**, *36*, e6570. [[CrossRef](#)]
29. Wei, C.; Sun, B.; Zhao, Z.; Cai, Z.; Liu, J.; Tan, Y.; Wei, H.; Liu, Z.; Bian, Z.; Huang, C. A Family of Highly Emissive Lanthanide Complexes Constructed with 6-(Diphenylphosphoryl)Picolinate. *Inorg. Chem.* **2020**, *59*, 8800–8808. [[CrossRef](#)]
30. Van den Hende, J.R.; Hitchcock, P.B.; Holmes, S.A.; Lappert, M.F.; Leung, W.-P.; Mak, T.C.W.; Prashar, S. Synthesis and Characterisation of Lanthanide(II) Aryloxides Including the First Structurally Characterised Europium(II) Compound [Eu(OC₆H₂bu^t₂-2,6-Me-4)₂(thf)₃·thf (thf = tetrahydrofuran)]. *J. Chem. Soc. Dalton Trans.* **1995**, 1427–1433. [[CrossRef](#)]
31. Barnhart, D.M.; Clark, D.L.; Gordon, J.C.; Huffman, J.C.; Vincent, R.L.; Watkin, J.G.; Zwick, B.D. Synthesis, Properties, and X-Ray Structures of the Lanthanide η⁶-Arene-Bridged Aryloxide Dimers Ln₂(O-2,6-*i*-Pr₂C₆H₃)₆ and Their Lewis Base Adducts Ln(O-2,6-*i*-Pr₂C₆H₃)₃(THF)₂ (Ln = Pr, Nd, Sm, Gd, Er, Yb, Lu). *Inorg. Chem.* **1994**, *33*, 3487–3497. [[CrossRef](#)]
32. Thornton, D.A. Crystal Field Aspects of the Vibrational Spectra of Metal Complexes. *Coord. Chem. Rev.* **1984**, *55*, 113–149. [[CrossRef](#)]

33. Galyametdinov, Y.; Athanassopoulou, M.A.; Griesar, K.; Kharitonova, O.; Soto Bustamante, E.A.; Tinchurina, L.; Ovchinnikov, I.; Haase, W. Synthesis and Magnetic Investigations on Rare-Earth-Containing Liquid Crystals with Large Magnetic Anisotropy. *Chem. Mater.* **1996**, *8*, 922–926. [[CrossRef](#)]
34. Luo, Y.; Han, Y.; Lin, J. Synthesis and Luminescent Properties of Europium (III) Schiff Base Complexes Covalently Bonded to Silica Xerogels. *J. Lumin.* **2007**, *122–123*, 83–86. [[CrossRef](#)]
35. Gagne, O.C.; Hawthorne, F.C. Empirical Lewis Acid Strengths for 135 Cations Bonded to Oxygen. *Acta Crystallogr. Sect. B* **2017**, *73*, 956–961. [[CrossRef](#)] [[PubMed](#)]
36. Moehring, S.A.; Miehlisch, M.; Hoerger, C.J.; Meyer, K.; Ziller, J.W.; Evans, W.J. A Room-Temperature Stable Y(II) Aryloxide: Using Steric Saturation to Kinetically Stabilize Y(II) Complexes. *Inorg. Chem.* **2020**, *59*, 3207–3214. [[CrossRef](#)] [[PubMed](#)]
37. Spinner, E.; Late, A.B. The Electronic Spectra of Acetophenones Substituted in the Methyl Group. *Spectrochim. Acta* **1961**, *17*, 558–567. [[CrossRef](#)]
38. Rowe, W.F.; Marginean, I.; Carnes, S.; Lurie, I.S. The Role of Diode Array Ultraviolet Detection for the Identification of Synthetic Cathinones. *Drug Test. Anal.* **2017**, *9*, 1512–1521. [[CrossRef](#)]
39. Berger, J.; Staretz, M.E.; Wood, M.; Brettell, T.A. Ultraviolet Absorption Properties of Synthetic Cathinones. *Forensic Chem.* **2020**, *21*, 100286. [[CrossRef](#)]
40. Becke, A.D. Density-Functional Thermochemistry. III. The Role of Exact Exchange. *J. Chem. Phys.* **1993**, *98*, 5648–5652. [[CrossRef](#)]
41. Tomasi, J.; Mennucci, B.; Cammi, R. Quantum Mechanical Continuum Solvation Models. *Chem. Rev.* **2005**, *105*, 2999–3094. [[CrossRef](#)] [[PubMed](#)]
42. Wu, Y.; Yu, H.; Guo, Y.; Zhang, Y.; Jiang, X.; Sun, B.; Fu, K.; Chen, J.; Qi, Y.; Zheng, J.; et al. Promoting Hydrogen Absorption of Liquid Organic Hydrogen Carriers by Solid Metal Hydrides. *J. Mater. Chem. A* **2019**, *7*, 16677–16684. [[CrossRef](#)]
43. Zheng, X.; Li, G.; Guo, Y.; Yu, H.; Li, S.; Xiao, R.; Zheng, J.; Li, X. Yttrium Trihydride Enhanced Lithium Storage in Carbon Materials. *Carbon* **2020**, *164*, 317–323. [[CrossRef](#)]
44. Frisch, M.J.; Trucks, G.; Schlegel, H.B.; Scuseria, G.E.; Robb, M.A.; Cheeseman, J.; Scalmani, G.; Barone, V.; Mennucci, B.; Petersson, G.A.; et al. *Gaussian 09 Revision A.1*; Gaussian Inc.: Wallingford, CT, USA, 2009.
45. Reed, A.E.; Curtiss, L.A.; Weinhold, F. Intermolecular Interactions from a Natural Bond Orbital, Donor-Acceptor Viewpoint. *Chem. Rev.* **1988**, *88*, 899–926. [[CrossRef](#)]

Disclaimer/Publisher's Note: The statements, opinions and data contained in all publications are solely those of the individual author(s) and contributor(s) and not of MDPI and/or the editor(s). MDPI and/or the editor(s) disclaim responsibility for any injury to people or property resulting from any ideas, methods, instructions or products referred to in the content.